Orientational order in dense molecular hydrogen: A first-principles path-integral Monte Carlo calculation

Efthimios Kaxiras and Zhian Guo

Department of Physics and Division of Applied Sciences, Harvard University, Cambridge, Massachusetts 02138

A quantum-mechanical simulation of orientational order in solid molecular hydrogen is presented, based on path-integral Monte Carlo calculations. The effective potential between nearest-neighbor hydrogen molecules is derived from first-principles total energy calculations, taking full account of the symmetries of the Hamiltonian within a hexagonal close-packed arrangement of the molecule centers. A first-order orientational order transition is found by studying short- and long-range angular correlations and the behavior of the corresponding order parameters. A pressure-temperature phase diagram is constructed and compared to relevant experimental and theoretical results.

I. INTRODUCTION

The various phases of solid hydrogen have been the subject of extensive experimental and theoretical studies.[1] In the last few years interest in the high-pressure behavior of this system was renewed, due to the development of diamond anvil cells that can reach pressures in the Mbar (1 Mbar = 100 GPa) range.[2] The motivation for these studies is the quest to observe the insulator-to-metal transition postulated by Wigner and Huntington:[3] A sufficiently large pressure (predicted to be ~ 3 Mbar)[4] is expected to turn the insulating molecular phase to a metallic atomic phase. The possibility of superconductivity in the high-pressure phase, predicted by Ashcroft,[5] and estimated to take place near room temperature,[6-8] gave additional impetus to the study of solid hydrogen. Only recently, Silvera and collaborators[9-13] and Mao and collaborators[14-20] have achieved in the laboratory the required pressures (1-2 Mbar) to observe such phenomena. These experimental studies showed that the highly compressed molecular phase of hydrogen is a fascinating phase in itself, with a rich phase diagram which possibly includes a metallic phase, even before the molecular-to-atomic transition takes place.

From the theoretical point of view, one of the major difficulties in obtaining a realistic description of hydrogen at these pressures is the quantum nature of the protons: The zero-point motion associated with the proton degrees of freedom makes it necessary to treat them as quantum rather than classical particles.[4] This complicates enormously the standard electronic structure approach used to describe the physics of solids, which is based on a classical treatment of the ionic degrees of freedom. In this paper we discuss a methodology for studying the physics of solid hydrogen in the molecular phase, using realistic interactions between the protons derived from extensive first-principles calculations, and taking account of the quantum nature of rotational degrees of freedom through path-integral Monte Carlo (PIMC) simulations.

The paper is organized as follows: Section II describes the derivation of a realistic interaction Hamiltonian for the molecular solid by fitting static first-principles calculations. Section III describes the PIMC simulations and the observed order-disorder transition. Section IV contains a study of the pressure dependence of the transition temperature. Finally, Sec. V discusses the limitations of this approach and gives a comparison to relevant experimental and theoretical work.

II. DERIVATION OF REALISTIC PROTON INTERACTIONS

In the pressure range that we will discuss, we will assume that hydrogen remains in the molecular phase. The justification for this assumption comes both from experiment and from theory. Experimental results show that there is a well-defined mode corresponding to intramolecular vibrations in solid hydrogen (called a vibron).[10,11,14-16] The frequency of this mode has been measured experimentally as a function of pressure. The vibron frequency first increases with applied pressure and eventually starts to decrease.[13-15] These changes in frequency, although quite pronounced, are such that they keep the vibron mode (with frequency in the 4000 cm^{-1} range) clearly separated from intermolecular vibrations, which have much lower frequencies (below 1000 cm^{-1}). This is strong indication that the molecular nature of the solid remains intact to a very high pressure. Abrupt changes in the vibron frequency have been interpreted as indications of phase transitions and possibly of qualitative changes in the electronic spectrum.[10,16-18]

At low densities, molecular hydrogen has a large gap in the electronic spectrum, separating bonding from antibonding states. Ashcroft has discussed how the structure of the solid can influence the nature of electronic states.[21] Indeed, detailed theoretical studies show that the electronic gap is sensitive to the density,[22-24] as well as the bond length and the orientation of the hydrogen pairs,[25,26] and can vanish when these parameters are varied. An example is shown in Fig. 1, where the band gaps of two different ordered structures are compared as a function of relative molar density (normalized to its
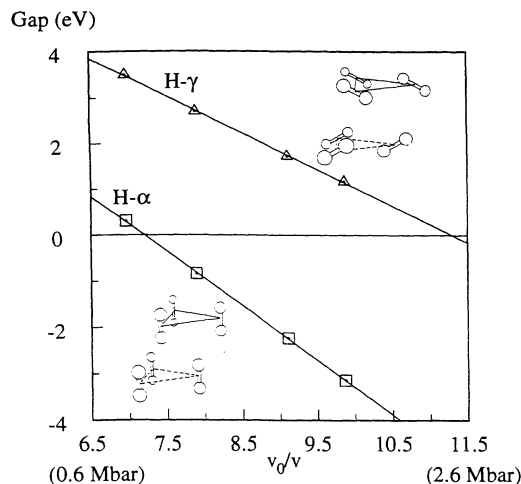
Gap (eV)

FIG. 1. Electronic gap (in eV) vs relative density for the H-α and H-γ structures (shown schematically as insets). v_0 is the zero-pressure volume. The corresponding pressure range (using the experimental EOS; see text) is given in parentheses.

zero-pressure value). As this figure shows, certain ordered structures (e.g., the H-γ structure) maintain a clear separation (band gap) between bonding and antibonding electronic states up to very high densities or pressures, if one uses an equation of state to translate density to pressure (see details below). Furthermore, previous studies have revealed that the configurations with larger band gap are also the energetically favored ones.[25] When the bonding and antibonding manifolds of electronic states are clearly separated in energy (the band gap is positive), one can think of the two electrons associated with each H_2 pair as belonging to the intramolecular bond, in which case a molecular picture of the solid is meaningful. When the gap vanishes the molecular picture begins to lose its physical meaning, since the antibonding states start being occupied and the electrons acquire metallic character. At still higher pressure, the vibron frequency is expected to become comparable to other vibrational modes in the crystal at which point the molecules will dissociate.[27] A recent simulation of the system treating the protons as classical point particles has revealed interesting changes in the structure and the dimensionality during the molecular-to-atomic transition.[28]

Having established the plausibility of the molecular picture for pressures in the 1–2 Mbar range, we then consider a simplified model for the motion of protons. All hydrogen atoms are paired to form molecules, which have six independent ionic degrees of freedom associated with the presence of two protons. Experiment indicates that as the pressure increases the molecules form a hexagonal close packed (hcp) lattice, and there is indirect evidence that this lattice structure persists in the 1–2 Mbar pressure range.[18] The pair of hydrogen atoms constituting a molecule can be thought of as a dumbbell, with an average length which depends on the pressure. We take the average pressure-dependent dumbbell length to be the equilibrium bond length of hydrogen molecules as obtained from previous total-energy calculations.[25] We

also use the results of those calculations to determine the optimal c/a ratio of the hcp lattice. This structural parameter tends to decrease with increasing pressure for the low-energy ordered configurations (such as H-γ),[25] in accordance with experimental measurements.[29] In contrast, the higher-energy H-α structure prefers a larger c/a ratio with increasing pressure.[25]

With fixed molecule lengths and fixed molecule centers at hcp lattice sites, there remain only two rotational degrees of freedom for each molecule, the θ and ϕ angular coordinates. Here we do not take the nuclear spin explicitly into account. Thus, no distinction is made between ortho (total nuclear spin 1) and para (total nuclear spin 0) hydrogen molecules. At the pressure range we will investigate, this distinction does not appear to be important,[10,14] and can therefore be neglected. We have performed extensive total-energy calculations in the space of the two angular coordinates using density functional theory in the local density approximation[30,31] (LDA) with a plane wave basis with an energy cutoff up to 52 Ry, and a dense grid of 144 points in the full Brillouin zone of the hcp lattice. Our total-energy studies show that the θ variable is associated with a much larger constant of rotation: Changes in θ orientation produce energy variations several (approximately 5) times larger than the energy variations corresponding to ϕ motion. This is demonstrated in Fig. 2 for molar volume 3.3 cm^3/mol. We notice that the barrier between $\theta = 60°$ and $\theta = 120°$ is only a factor of 2 larger than the energy barrier for ϕ motion, but due to the symmetry of the H_2 molecule (the two protons are equivalent), these two configurations can be viewed as having the same θ coordinate and ϕ coordinates differing by 180°. Thus, the energy variation in θ (for fixed ϕ) can be represented by an expansion

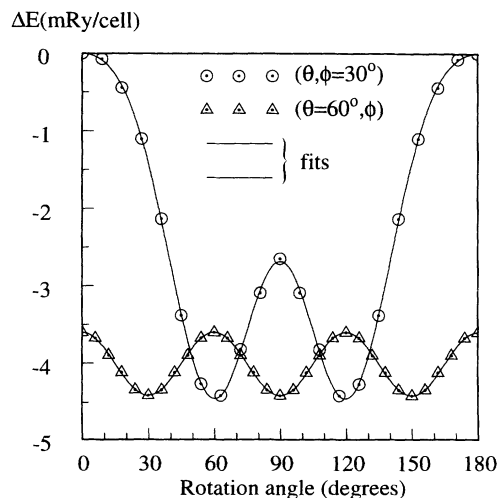$$V_0(\theta) = B_2 \cos(2\theta) + B_4 \cos(4\theta) + \cdots, \qquad (1)$$

ΔE(mRy/cell)

FIG. 2. Energy variations associated with rotations in the polar coordinate θ at fixed $\phi = 30°$ (circles) and the azimuthal coordinate ϕ at fixed $\theta = 60°$ (triangles). The solid lines are fits to the calculated values as described in the text.

which provides an excellent fit to the calculated values with the first four terms (see Fig. 2). It is physically plausible that if the V_0 potential has deep minima the θ variable will be restricted to values close to its equilibrium (i.e., $\theta_0 = 60°$ or equivalently 120°). Restricting θ to this value allows for a significant simplification of the problem, both at the level of calculating energy differences within the first-principles formalism (by reducing the number of configurations required to determine the parameters in the Hamiltonian), and at the level of performing finite-temperature quantum simulations (by allowing for much longer runs which reduce statistical fluctuations). In order to make the calculations tractable at both levels, we will assume that $\theta = \theta_0$ for all molecules. We shall critically examine the effect of this approximation, first, by comparing the relevant values of coefficients in the various potential-energy terms (below, in this section) and second, by considering the effect of this constraint on the potential energy surface for a particular case (in Sec. V). With this restriction in θ, only one degree of freedom is left for each molecule, the variable ϕ. This system is described by the following Hamiltonian:

$$\mathcal{H} = -D \sum_i \frac{1}{\sin^2 \theta_0} \frac{\partial^2}{\partial \phi_i^2} + \sum_n \sum_{i_1 < i_2 < \cdots < i_n} V_n(\phi_{i_1}, \phi_{i_2}, ..., \phi_{i_n}). \quad (2)$$

$\mathcal{H}$ contains the kinetic energy associated with each ϕ variable and the potential energy which includes all possible n-body interactions. Here $D = \hbar^2/(m_p d_e^2)$, m_p is the mass of the proton and d_e is the pressure-dependent equilibrium length of the molecule. We have found that by retaining only the two lowest-order n-body interactions ($n = 1$ and $n = 2$) in the Hamiltonian $\mathcal{H}$ we can obtain a very reasonable representation of the proton interactions.

The $n = 1$ interaction term obeys the symmetries of the underlying lattice, which for hcp gives the form

$$V_1(\phi) = A_6 \cos(6\phi) + A_{12} \cos(12\phi) + \cdots . \quad (3)$$

The coefficients A_6, A_{12}, etc., can be found by calculating the energy of ordered structures in which all molecules are rotated by exactly the same amount in ϕ with all other coordinates held fixed. We have performed such calculations and found that to an excellent approximation only the first term (A_6) is needed, with the other coefficients being at least two orders of magnitude smaller, for all the densities we considered. In Fig. 2 we show a typical fit to the calculated energies using the $\cos(6\phi)$ term alone. In the following we refer to this term as the "crystal field," since it describes the energetics of configurations that do not break the periodicity of the underlying hcp lattice.

The $n = 2$ interaction term in its most general form can be expressed as an expansion in spherical harmonics:

$$V_2 = \sum_l C_l \sum_{l_1, l_2, m_1, m_2} \begin{pmatrix} l_1 & l_2 & l \\ m_1 & m_2 & m \end{pmatrix}$$

$$\times Y_{l_1,m_1}(\Omega_1) Y_{l_2,m_2}(\Omega_2) Y_{l,m}^*(\Omega), \quad (4)$$

where $(m + m_1 + m_2) = 0$, $\Omega_1 = (\theta_0, \phi_1)$, $\Omega_2 = (\theta_0, \phi_1)$ describe the orientation of two molecules and $\Omega = (\theta, \phi)$ is the orientation of the vector connecting their centers, in a given coordinate frame.[32] Because of the inherent symmetry in the molecules (the two protons are equivalent), l_1 and l_2 must both be even. Furthermore, if either of them is zero, the corresponding term contains only one ϕ_i variable, and should be included in the V_1 term of the potential energy. Thus, the lowest-order terms in V_2 are

$$V_2 = \sum_{l=0,2,4} C_l \sum_{m_1, m_2} \begin{pmatrix} 2 & 2 & l \\ m_1 & m_2 & m \end{pmatrix}$$

$$\times Y_{l_1,n}(\Omega_1) Y_{l_2,m}(\Omega_2) Y_{l,m}^*(\Omega). \quad (5)$$

In principle, the range of interactions in V_2 is unlimited. In practice, we have found it convenient and adequate to keep only first-neighbor interactions.

In order to make the physical meaning of these terms more obvious, we have rewritten the $l = 0$ term as

$$f_0 = \frac{Q_{\alpha\beta}^{(1)} Q_{\beta\alpha}^{(2)}}{6r^5} \quad (6)$$

and the $l = 4$ term as

$$f_4 = \left(\frac{Q_{\alpha\beta}^{(1)} Q_{\alpha\beta}^{(2)}}{6r^5} - \frac{5Q_{\alpha\beta}^{(1)} Q_{\beta\alpha}^{(2)} r_\alpha r_\beta}{3r^7} + \frac{35 Q_{\alpha\beta}^{(1)} Q_{\gamma\delta}^{(2)} r_\alpha r_\beta r_\gamma r_\delta}{12r^9} \right), \quad (7)$$

where $Q_{\alpha\beta}^{(i)} = d_\alpha^{(i)} d_\beta^{(i)}$ with $\hat{\mathbf{d}}^{(i)} (i = 1, 2)$ the unit vector describing the orientation of molecule (i) and $\mathbf{r}$ the vector joining the centers of the molecules (1) and (2). In the above expressions the Greek letter indices correspond to Cartesian components of the vectors. The coefficient of f_0 is typically one order of magnitude smaller than the coefficient of f_4. This last term, which is the most important term in the Hamiltonian, is essentially the quadrupole-quadrupole interaction, as would be expected for neutral homopolar molecules. This interaction is believed to be responsible for the ordered low-pressure and low-temperature structure of solid molecular hydrogen, the $Pa3$ lattice.[1] Here we will demonstrate through careful fitting to first-principles results that the same type of interaction is important at high pressure. Furthermore, we will establish the relative magnitude of the different terms in this interaction which depend on the volume (see below).

The coefficients C_0, C_2, C_4 can be determined by considering molecule rotations that break the hcp lattice periodicity. Two such types of rotations are illustrated in Fig. 3. The first type [Fig. 3(a)] determines the values of C_l for interactions between out-of-plane nearest neighbors in the hcp lattice (denoted below as C_{l-o}), while the second type [Fig. 3(b)] determines the values of C_l for interactions between in-plane nearest neighbors (denoted as C_{l-i}). Before determining the values of C_{l-o} and C_{l-i}, the relevant crystal field contributions need to be subtracted from the total energy. We have performed extensive first-principles calculations of the energetics of such
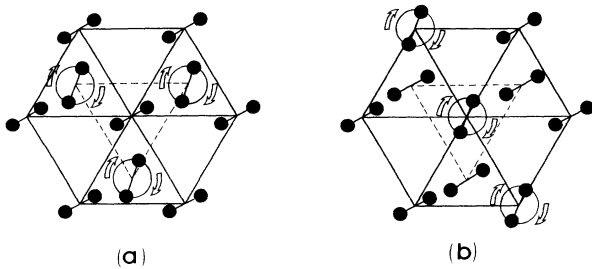
FIG. 3. Molecular configurations used to calculate the different terms in the Hamiltonian. The solid lines join centers of molecules that lie on one plane of the hcp lattice; the dashed lines join centers of molecules that lie on the next plane along the c axis. The curved arrows illustrate the motion of the molecules considered in the calculations: (a) motion that determines the out-of-plane coupling constants; (b) motion that determines the in-plane coupling constants.

FIG. 5. The behavior of the leading terms in the crystal field A_6 (triangles), the in-plane nearest-neighbor interaction C_{4-i} (circles), and the out-of-plane interaction C_{4-o} (squares), as a function of molar volume. The lines are fits to the calculated points. The solid circles are the two lowest-order terms in the polar angle potential V_0.

rotations at various densities. We find that in general the coefficients C_0, C_2 are much smaller in magnitude than C_4. In particular, C_2 is within the numerical noise of our first-principles calculations, and we opted to neglect this term.

Figure 4 shows the energy variations for rotations that determine the coefficients C_{4-i} (the in-plane nearest-neighbor interaction) and C_{4-o} (the out-of-plane nearest-neighbor interaction) at a specific volume (3.3 cm^3/mol). The energy variation due to the V_2 term alone is shown here, after the contribution of the crystal field has been subtracted out. The fits obtained by the expansion in Eq. (5) are rather satisfactory, given that the accuracy of the first-principles calculations is of order 1 mRy/unit cell. Figure 5 shows the dependence of the various coefficients on the volume. We used simple smooth curves
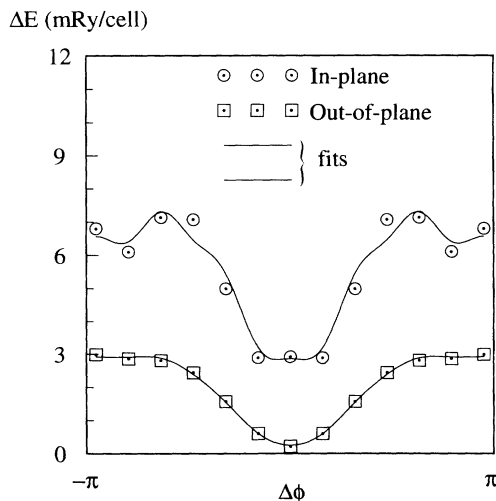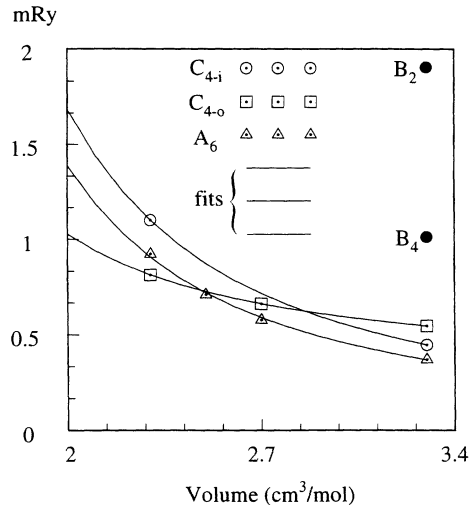

FIG. 4. Total energy vs azimuthal angle ϕ for molecular motions that determine the in-plane (dots) and out-of-plane (squares) coupling constants in the V_2 term of the Hamiltonian. The solid lines are fits to the calculated values as described in the text. The crystal field component V_1 has been subtracted out from the total energy. The in-plane results have been shifted by 3 mRy/cell for clarity.

to fit the calculated values, so that simulations could be performed at any volume in the interval between 2.3 and 3.3 cm^3/mol. As expected, all coefficients decrease with increasing volume because the separation between molecules becomes larger and the intermolecular interactions weaker. In this figure we also display the two lowest-order coefficients in the expansion V_0, Eq. (1), at volume 3.3 cm^3/mol. The leading term in this expansion (B_2) is much larger (by about a factor of 5) than the coefficients of other terms in the potential (A's and C's), indicating the large variation in the energy with the polar angle θ that was discussed earlier. It is also noteworthy that the energy variation due to changes in the polar angle becomes much more pronounced at lower volumes (higher pressures), as was established by earlier calculations.[26] Consequently, we expect the V_0 term to increase faster than the other terms. This supports the approximation of restricting the polar angle θ to its equilibrium value.

Through this analysis, we have then obtained a Hamiltonian that describes the energetics of molecular motion in solid hydrogen as an expansion in nearest-neighbor interactions that obey the proper symmetries. Since these interactions reproduce the results of first-principles calculations with an accuracy comparable to the error bars in such calculations, the Hamiltonian can be viewed as a first-principles description of the system *for the types of motion considered here*. We emphasize this last point, because our Hamiltonian will be able to capture neither the molecular-to-atomic transition nor the metallic molecular phases. Both of these situations are expected to be important near the high end ($\sim$ 2 Mbar) of the pressure range we considered. Finally, all the structures we have considered in the LDA calculations have nonvanishing band gaps for the range of volumes under investigation.

Thus, the relative energies that determine the coefficients of the Hamiltonian are not affected by the well known deficiency of the LDA to reproduce the magnitude of the electronic gap.[24]

III. PATH-INTEGRAL SIMULATIONS

With our interaction Hamiltonian we proceeded to perform simulations that take into account the quantum nature of the rotational degrees of freedom (the ϕ's). The simulations are based on Feynman's path-integral formulation for the propagator[33]

$$P(x_1, x_2; \beta) = \langle x_1 | e^{-\beta \mathcal{H}} | x_2 \rangle, \qquad (8)$$

which in imaginary time $\tau = i \frac{\beta \hbar}{N}$ becomes

$$P(x_1, x_2; \beta) = \left(\frac{mN}{2\pi \hbar^2 \beta} \right)^{N/2} \int [dx] e^{-S}, \qquad (9)$$

with the action S defined by

$$S = \frac{1}{\hbar} \int_0^{\beta \hbar} \left[\frac{m}{2} \left(\frac{dx}{d\tau} \right)^2 + V(x) \right] d\tau. \qquad (10)$$

The integration $\int [dx]$ is over all possible paths with end points (x_1, x_2). m is the mass of the particles in the system and N is a large number of intervals into which the inverse temperature β (or imaginary time $i\beta\hbar$) is discretized. Equation (10) is formally equivalent to the partition function of a system consisting of N beads,[34] interacting by harmonic springs of constant $mN/(\hbar^2 \beta^2)$ in an external potential $(1/N)V(x)$. For our system each coordinate x represents a collective set of variables $\{\phi_i\}$, while the mass of these particles is $(2D/\sin^2 \theta_0)^{-1}$.

We use the standard Metropolis algorithm to sample the propagator $P(x, x; \beta)$ through a Monte Carlo procedure, which then gives the probability distribution of the variables $\{\phi_i\}$ at a given reduced temperature β^{-1} and density (the density determines the values of the coefficients $A_6, C_{4-i}, C_{4-o}, \dots$ which describe the external potential for the variables $\{\phi_i\}$). We use $N = 40$ beads and sample the system for 2×10^5 MC moves per bead (10^4 MC moves per bead were used for thermalization). We performed calculations for a system of 64 molecules arranged in an hcp supercell of four planes with 16 molecules on each, and having periodic boundary conditions. We have implemented the calculation on a parallel processor computer (CM-2) but found that the use of parallelism was of limited help. This is because a mixture of local and global MC moves was necessary for effective sampling of phase space. Global moves are ideally suited for a parallel architecture, whereas local moves are inefficient. The optimal ratio of global to local moves (determined by experimentation) was 1:50, which makes this particular system a poor choice for parallel computations.

We examined a range of volumes from 2.3 to 3.3 cm^3/mol. In order to translate these volumes to pressure,

we used both an experimental[36] equation of state (EOS) and a theoretically obtained EOS. These are compared in Fig. 6. The theoretical EOS obtained from our calculations lies below the experimental one, because it is based on static calculations which do not take into account zero-point vibrational and rotational motion. When the protons are treated quantum mechanically the theoretical EOS is shifted to higher pressure values.[4,22] As seen from Fig. 6, the range of volumes we considered corresponds to pressures of 0.55–1.60 Mbar (using the theoretical EOS), or 0.75–1.86 Mbar (using the experimental EOS).[36] For each volume we calculated the properties of the system at various temperatures. The main result of these simulations is that there exist two clearly distinguishable phases of the system: an orientationally ordered phase below some pressure-dependent transition temperature T_c and an orientationally disordered phase above this temperature. The terms "orientational order" and "orientational disorder" refer to the azimuthal angles ϕ_i, which are the only variables in the Hamiltonian [see Eq. (2)]. For clarity, we will name these phases azimuthally ordered phase (AOP) and azimuthally disordered phase (ADP). A picture of the two phases can be obtained by superimposing several instantaneous configurations selected among the large number of MC steps of each run. Figure 7 shows such superpositions of equal numbers of instantaneous configurations for the case of (a) $T < T_c$ and (b) $T > T_c$; there is an obvious qualitative difference between the two cases, which allows us to label them "ordered" and "disordered" respectively. The precise ordering scheme in the AOP, the nature of the ADP, and the nature of the transition all show interesting features which we discuss below.

In order to describe the system in the AOP and ADP we first measured the correlations between nearest-neighbor *relative* orientations. To this end, we defined a
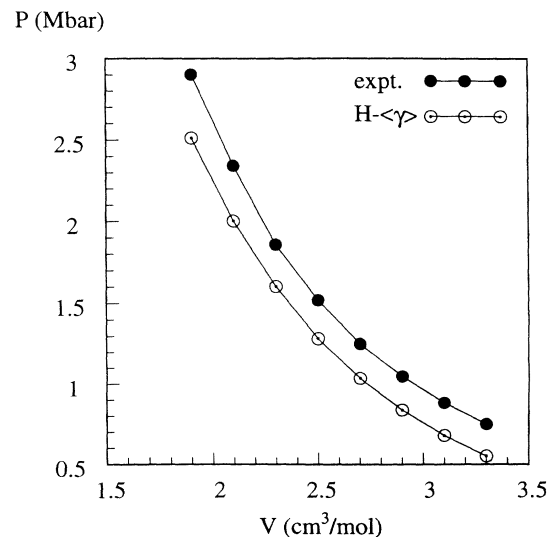

FIG. 6. Experimental (Ref. 36) (dots) and theoretical (circles) equations of state for molecular hydrogen. The theoretical EOS is an average over low-energy structures with polar angle $\theta = 60°$.
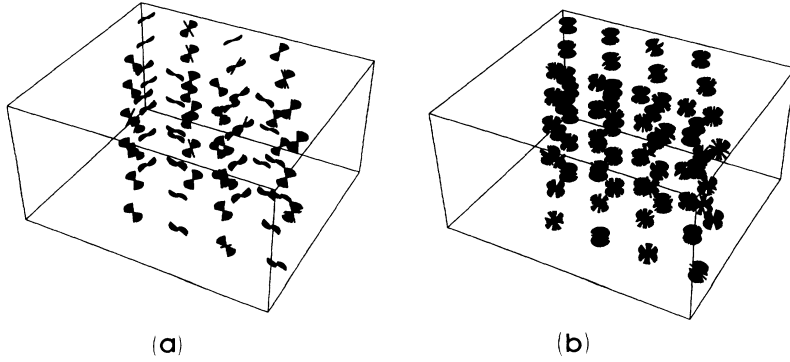
FIG. 7. Superpositions of instantaneous configurations of molecules from typical PIMC simulations: (a) the azimuthally ordered phase; (b) the azimuthally disordered phase.

set of six neighbors for any given molecule (labeled 0 in Fig. 8), three of them in the plane (labeled 1–3), and three out of plane (labeled 4–6). This assignment allows one to sweep over all the nearest-neighbor relative orientations as the label 0 is successively attached to every molecule in the system. The calculated distributions of the nearest-neighbor relative orientations for $T < T_c$ and $T > T_c$ are shown in Fig. 9. For $T < T_c$ both the in-plane and out-of-plane correlations reveal the presence of short-range order (SRO). The ordering scheme is illustrated in Fig. 8. For convenience, we attach arrows to the lines that represent the molecules, so that we can discuss the ordering in terms of spins that can be "parallel" or "antiparallel." The arrows point to the atom in each molecule which lies above the ab plane. This assignment is possible because the polar angle is kept fixed at $\theta_0 = 60°$. As seen in Fig. 8, neighbor 1 is parallel to 0, whereas neighbors 2 and 3 are at angles $\pm\pi/3$. The existence of two peaks is due to the fact that when the label 0 is placed at one of the sites labeled 2 or 3 in Fig. 8, the sign of the relative orientation changes. Similarly, neighbors 4 and 5 are antiparallel to the molecule at the origin, while neighbor 6 is at a relative angle of $\pm 2\pi/3$. Again, the two peaks in the distribution of the relative orientation of 0 and 6 are due to the fact that when label 0 is placed to the site labeled 6 in Fig. 8, the relative angle between the molecule at the new origin and at the

new site 6 has opposite sign than before. The width of the peaks is independent of the temperature and is due to quantum fluctuations. These fluctuations are evident in the representation of the ordered phase in Fig. 7(a). The smooth distribution of points in Fig. 9 for $T < T_c$ indicates that our PIMC results are well converged in terms of sampling of MC moves. We have found that the PIMC data of Fig. 9 for $T < T_c$ fall on perfect Gaussian curves, centered at the values described above, with a half-width equal to $\sim \pi/4$.

Another way of revealing the presence of SRO is through the order parameters

$$\mathcal{S}_I = \frac{1}{2} \sum_{i=1,2,3} \langle \cos(\phi_i - \phi_0) \rangle, \tag{11}$$

$$\mathcal{S}_O = -\frac{2}{5} \sum_{i=4,5,6} \langle \cos(\phi_i - \phi_0) \rangle, \tag{12}$$
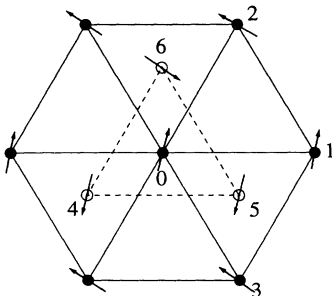

FIG. 8. The ordering pattern in the azimuthally ordered phase. The six in-plane nearest neighbors (dots connected by solid lines) and the three out-of-pane nearest neighbors (circles connected by dashed lines) of the central molecule labeled 0 are shown. The arrow heads indicate the position of the atoms that lie above the ab plane of the hcp lattice. The view is along the c axis. The labels 1–6 identify the different types of neighbors (see text).
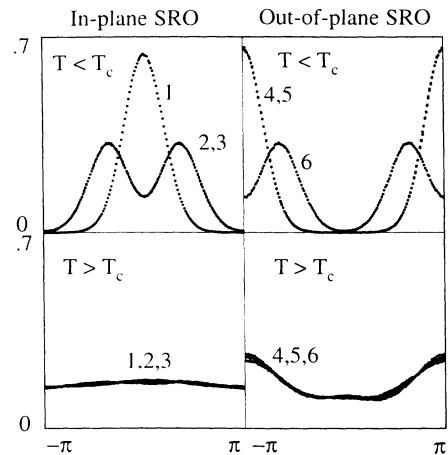

FIG. 9. Short-range order as revealed by nearest-neighbor correlations between any given molecule and its neighbors labeled 1–6 shown in Fig. 8: in-plane (left two panels), out-of-plane (right two panels), below T_c (top two panels), and above T_c (bottom two panels); T_c is the transition temperature for ordering. The various peaks correspond to the ordering scheme of Fig. 8. The widths of the peaks are associated with quantum-mechanical fluctuations. Notice the non-vanishing out-of-plane correlations for $T > T_c$ (lower right panel), which signifies short-range order in the azimuthally disordered phase (see text).

with the position 0 sweeping through all sites in the system, and the sites $i = 1, \ldots, 6$ referring to the the nearest neighbors of each molecule, as identified in Fig. 8. The angular brackets denote an average over the simulation. The order parameters S_I and S_O measure the degree of SRO for in-plane and out-of-plane neighbors respectively, and are normalized so that a perfectly ordered classical system would give $S_I = S_O = 1$. Here (as well as in the long-range order parameter defined below) the standard $1/M$ normalization, where M is the number of molecules in the simulation cell, is implied. A plot of these order parameters at a particular volume, as a function of reduced inverse temperature, is shown in Fig. 10.

In addition to the SRO revealed by the relative orientations of nearest neighbors, there is long-range order (LRO) in the AOP. This is seen through the behavior of the order parameter

$$\mathcal{L} = \langle \cos 2(\phi_0 - \Phi_\lambda) \rangle, \tag{13}$$

where again the label 0 sweeps through all the lattice sites and the angular brackets indicate an average over the simulation. The angle ϕ_0 is the absolute angle describing the orientation of a given molecule with respect to the lattice. The label λ takes two values that correspond to the two possible orientations Φ_λ of molecules on a single plane in the ordering scheme shown in Fig. 8 (the sites 1 and 2, for example). The factor of 2 in the cosine of $\mathcal{L}$ is included so that one does not have to distinguish between alternate planes: Since the relative orientation of molecules on alternate planes in the AOP changes by π (see Fig. 8), this factor makes all contributions to the order parameter $\mathcal{L}$ have the same sign. Thus, $\mathcal{L}$ describes the absolute orientation of molecules with respect to the lattice. If all molecules are aligned in the same manner, the relative orientation between two molecules at any distance is fixed by their relative position on the lat-

FIG. 10. Behavior of the order parameters for long-range order $\mathcal{L}$ (dots), in-plane short-range order S_I (circles), and out-of-plane short-range order S_O (triangles) as a function of inverse temperature β. The abrupt change takes place at the same value of β for all three order parameters. Notice the nonvanishing value of S_O at high temperature (low β values). This calculation corresponds to volume 3.3 cm^3/mol.

tice. Consequently, if $\mathcal{L}$ acquires a nonvanishing value, the system has long-range order. The behavior of $\mathcal{L}$ as a function of reduced inverse temperature is shown in Fig. 10. The long-range order in the system disappears at the same temperature as the in-plane and out-of-plane short-range order. The ordered phase has the $Pca2_1$ symmetry, compatible with the results of Nagara and Nakamura,[35] who found a configuration of the same symmetry to be the lowest-energy ordered molecular structure within the LDA.

There is one feature of the behavior of the order parameters that is intriguing: While the values of S_I and $\mathcal{L}$ vanish above T_c (within statistical fluctuations), the value of S_O is not negligible in the ADP. This can also be seen in the behavior of the nearest-neighbor correlations for out-of-plane neighbors at $T > T_c$ (see Fig. 9). Apparently, in the ADP a non-negligible out-of-plane correlation is present, which tends to orient neighboring molecules on alternate planes at a relative angle equal to π. This observation strongly suggests that the ADP can be thought of as a phase with weak short-range correlations, which bears some resemblance to liquid crystal phases (see also Sec. V).

IV. TRANSITION TEMPERATURE vs PRESSURE

We studied the temperature dependence of the order parameters that describe SRO and LRO for the range of volumes discussed earlier. The results are shown in Figs. 11(a) and 11(b) for SRO (the in-plane and out-of-plane order parameters respectively) and in Fig. 11(c) for LRO. For all cases examined there is a transition temperature at which there is an abrupt change in the value of the order parameters. The transition temperature is the same, no matter which order parameter is used to define it, as in the case shown in Fig. 10. The main result of these studies is that the transition temperature increases monotonically with pressure. This is to be expected, since the interactions become stronger as the density increases (see Fig. 5) and more thermal energy is needed to destroy the order.

We comment briefly on the persistence of significant out-of-plane SRO in the disordered phase, and its dependence on temperature. The persistence of out-of-plane SRO in the ADP becomes less pronounced as the density increases: At the highest density (smallest volume) considered in Fig. 11(b), the SRO in the high-temperature phase disappears very quickly with increasing temperature. This behavior is expected, since at higher densities the transition temperature is also higher, so that when the system passes to the disordered phase the thermal energy is already high enough to destroy any remaining weak out-of-plane short range correlations.

In Fig. 12 we summarize the behavior of the transition temperature as a function of pressure. There are large error bars associated with the values of the transition temperature. These error bars arise from two sources. First, the determination of the transition temperature is uncertain: The jumps in the values of the order parame-
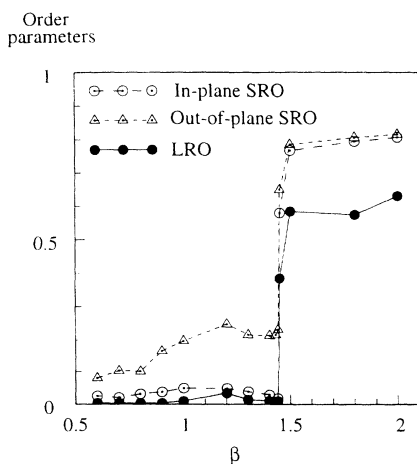
ters shown in Figs. 10 and 11 appear sharp when plotted against the reduced inverse temperature β but the corresponding value of T_c involves an uncertainty which is equal to the difference in the β^{-1} values between the two points closest to the jump. As the density increases, the transition becomes less abrupt (this is most noticeable in the lowest volume curves of Fig. 11). Thus, from the
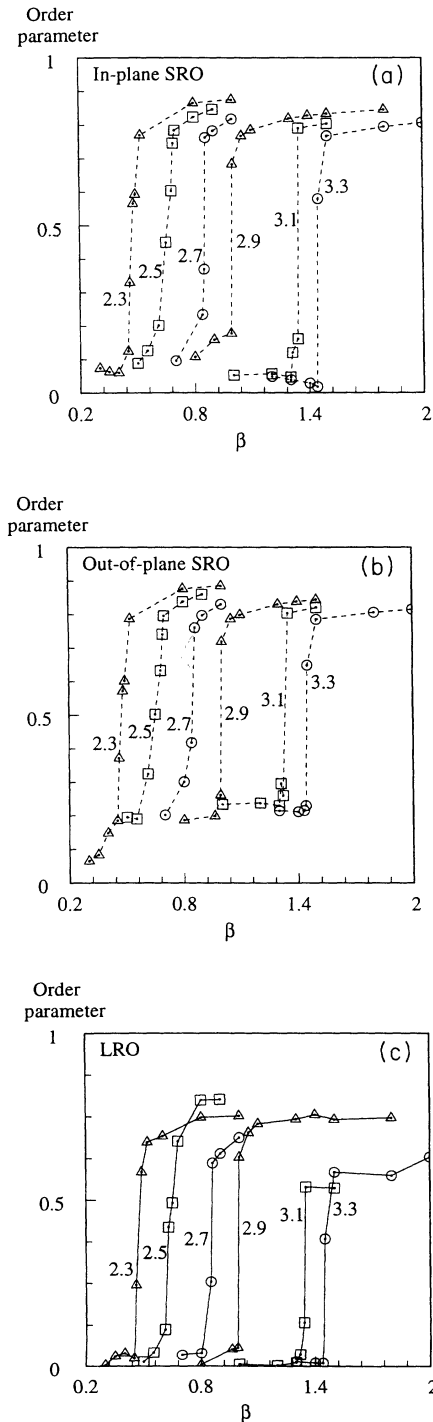

FIG. 11. Behavior of the (a) in-plane SRO, (b) out-of-plane SRO, and (c) LRO order parameters as a function of inverse temperature β, for the different volumes considered. Each curve is labeled by the corresponding volume in cm^3/mol.
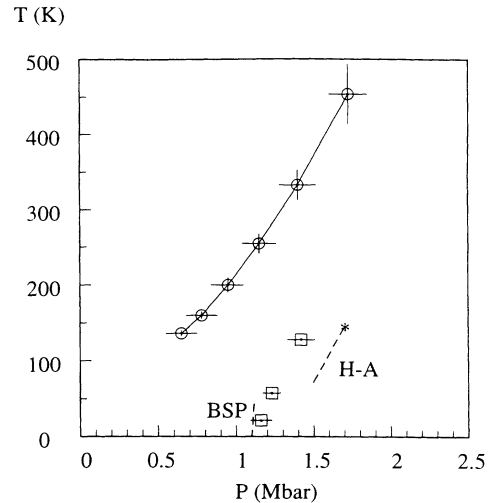

FIG. 12. Phase diagram for the AOP-ADP transition as calculated (circles). The solid line is guide to the eye. The temperature error bars come from the sharpness in the transition of the order parameter plots (see Fig. 11). The pressure error bars come from the uncertainty in the equation of state that was used to translate volume to pressure (see text). The squares are from the calculation of Runge et al. (Ref. 40) with error bars due to incomplete MC annealing. The experimentally known BSP and H-A transitions are shown as dashed lines. The asterisk marks the point where the H-A line appears to terminate, as measured by Raman scattering.

simulations alone, error bars in T_c that increase with the pressure are observed (see Fig. 12). This is a manifestation of finite-size effects which become more pronounced at higher pressure and temperature. A second source of uncertainty is our method of translating density to pressure: The experimental EOS is an extrapolation from low-pressure measurements.[36] It is not clear how reliable this equation is in the density range we are considering. A change in the structure and orientation of the molecules, which results in lower energy at compressed volumes, could produce significant deviations from the extrapolation of low-pressure experimental results. On the other hand, the theoretical EOS is obtained from static calculations and does not include zero-point motion. Thus, the experimental EOS probably overestimates the effect of zero-point motion, whereas the theoretical EOS underestimates it. In Fig. 12 we give the T_c vs P curve obtained from the average of the two EOS, while the pressure error bars indicate the difference between the two calculations.

V. DISCUSSION AND CONCLUSIONS

The potential energy of the Hamiltonian $\mathcal{H}$ of Eq. (2) is related to a class of classical spin models studied extensively in the literature.[37-39] The closest model to the system studied here is that discussed by Bruinsma and Nelson,[38] which included crystal field terms and nearest-neighbor interactions of the XY type $[\cos(\phi_i - \phi_j)$, which is contained in the f_0 term, Eq. (6)]. There are two important differences between that model and the Hamilto-

nian studied here: First, both the crystal structure and the nearest-neighbor interactions we considered are considerably more complicated than a simple XY model. Second, our model is a quantum-mechanical one, whereas the model studied by Bruinsma and Nelson is a classical one. Nevertheless, the behavior of the classical model contained much of the physical behavior we observed in the present model. A second-order phase transition was found by Bruinsma and Nelson between a smectic-C (tilted hexatic) and a stacked hexatic phase. These two phases are characterized by LRO and SRO of the in-plane orientations, whereas in our study we find phases characterized by the presence or absence of in-plane orientational order (both SRO and LRO). Thus, the smectic-C phase corresponds to the AOP described above, whereas the stacked hexatic phase corresponds to the ADP phase. Our numerical evidence suggests a first-order transition between the two phases, whereas Bruinsma and Nelson found a second-order transition in their classical model. The difference may be due to the complicated lattice structure of our model, which includes four sublattices and may have a multicomponent order parameter. The determination of the order parameter and the nature of the transition in the model Hamiltonian Eq. (2) deserve further theoretical analysis which is beyond the scope of the present work.

A more recent theoretical study by Runge et al.[40] reported PIMC calculations on solid molecular hydrogen at high pressures. The intermolecular interactions were based either on a pair potential fitted to dilute gas data, or to first-principles calculations for solid phases of molecular hydrogen in cubic lattices. There are several important differences between the present study and the work of Runge et al. First, different Hamiltonians were used in the simulations. We have restricted the phase space to the azimuthal angular coordinates of the molecules, whereas the potential energy of Runge et al. contains both angular coordinates for each molecule. Second, the interaction terms in our Hamiltonian incorporate explicitly all the proper symmetries of the hcp lattice, whereas Runge et al. have a general interaction term, the coefficients of which were fitted by performing first-principles calculations on fcc lattices. Third, both the molecular bond length and the c/a ratio of the hcp lattice were optimal for each volume in our calculations, while they were kept fixed at their ideal (zero-pressure) values in the study by Runge et al. As a consequence of these differences in the model, quite different behavior is obtained for the system. The results of the two calculations are compared in Fig. 12. We obtain significantly higher transition temperatures than Runge et al. We note that our error bars have a different origin than those reported by Runge et al. In particular, both the temperature and the pressure error bars in our study are independent of statistical errors, whereas Runge et al. attribute their error bars to imperfect MC annealing.[40] Our PIMC are long enough (see Sec. III) to essentially eliminate statistical errors. However, neither the temperature value nor the pressure value can be better determined by better statistics. The uncertainty in the temperature comes from a smoothing of the transition which is more

pronounced at higher temperatures and is the result of finite-size effects. The uncertainty in the pressure comes from using two different EOS for the system; at this point it is not clear which is a more realistic EOS at high pressure.

The most important restriction in the present simulation is that of the polar angle θ. As argued in Sec. II, this is a meaningful approximation for a strong polar confining potential. In Fig. 13 we show the confining potential for the polar angle, for a given azimuthal angle ($\phi = 30°$), and its ground state energy and wave function magnitude, obtained numerically by a quantum Monte Carlo method. The wave function magnitude is very strongly peaked in the region $60° < \theta < 120°$. In Fig. 14 we display the potential energy as a function of polar and azimuthal angles for the molecular hcp crystal. It is clear from this figure that the dependence of the potential on the azimuthal variable in the range of $60° < \theta < 120°$ is essentially the same as that for $\theta = 60°$, with small variations in the overall magnitude. Thus, restricting the variable θ to $60°$ exaggerates the strength of the azimuthal potential, without altering its shape. In this sense, inclusion of the polar angle as an independent variable would not alter the topology of the energy surface. Therefore, the effect of restricting the phase space of our Hamiltonian to one angular coordinate per molecule results in renormalization of the coupling constants, which displaces the ADP-AOP line away from its physical position. When additional degrees of freedom (such as the polar angles or the bond lengths) are taken into account explicitly, the coefficients in the V_1, V_2 terms will be renormalized to lower values and the contributions to the kinetic energy will increase. This will make it easier to remove the orientational order, thereby requiring higher pressure to restore order at fixed temperature, or less thermal energy to destroy order at fixed pressure. The net effect will be a shift of the AOP-ADP line toward higher pressure and lower temperature.

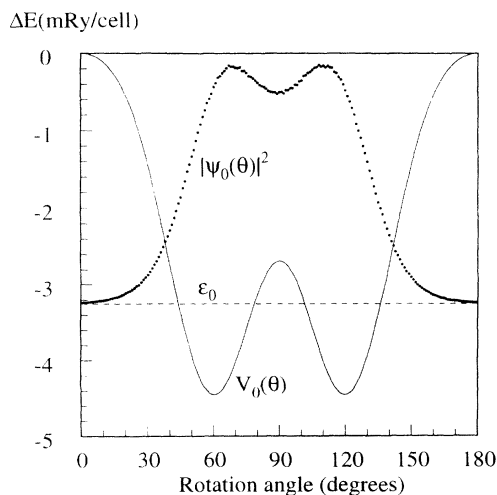Experimentally, at least two transitions between differ-

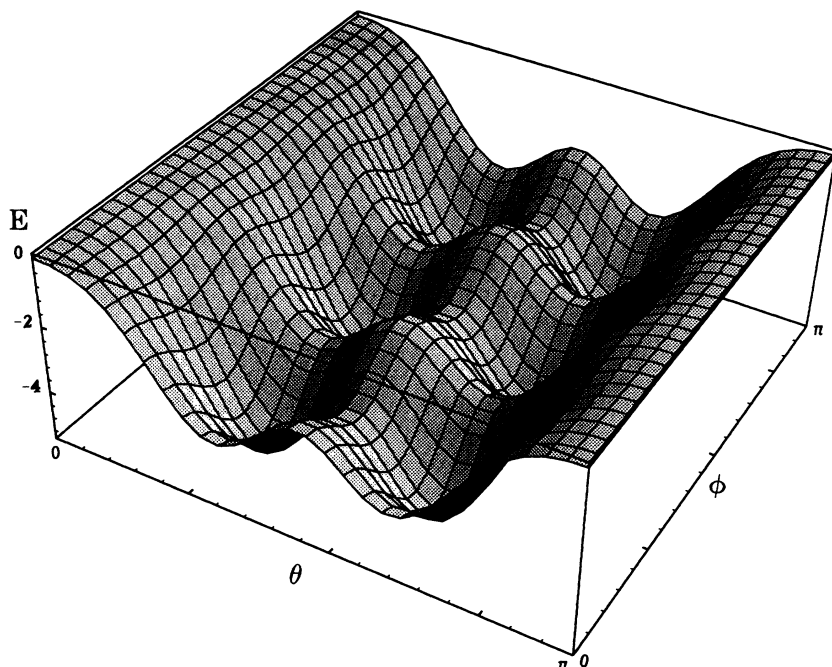FIG. 13. The energy and wave function magnitude of the ground state in the V_0 potential.

FIG. 14. A two-variable plot of the energy variation as a function of polar and azimuthal angles for the molecular hcp lattice at volume 3.3 cm^3/mol.

ent phases have been reported at pressures in the range between 1 and 2 Mbar for solid molecular hydrogen. One transition at 1.1 Mbar has been called the broken symmetry phase (BSP) transition, and a different one near 1.5 Mbar has been called the hydrogen-A (H-A) transition.[10] Both transitions are characterized by discontinuities in the vibron frequency. At low temperatures, the vibron frequency discontinuity is ~ 10 cm^{-1} for the BSP transition and much larger (~ 100 cm^{-1}) for the H-A transition. Moreover, the discontinuity exhibits interesting behavior at the H-A line: the vibron discontinuity as determined by Raman scattering disappears at approximately 1.7 Mbar and 140 K. The origin of the H-A transition is controversial,[12,41-43] and has been linked to the possible onset of metallic behavior in the system.[16,17,22,23,44] Additional transitions in this range cannot be ruled out.

As far as the ADP-AOP transition which we have described above is concerned, it cannot be unambiguously related to either the BSP or the H-A transitions. Both the BSP and the H-A transitions lie much below the line obtained in our simulations (see Fig. 12). Furthermore, the ADP-AOP transition we have described involves a symmetry breaking: In the ADP the symmetry is that of the hcp lattice whereas in the AOP a lower symmetry structure is found ($Pca2_1$). Silvera[45] has argued from general symmetry considerations that the H-A line should not involve a symmetry breaking transition if the line terminates at a critical point. This argument would preclude the identification of the AOP-ADP transition with the H-A line. However, recent experiments show that the infrared activity increases dramatically when the H-A line is crossed.[46] Although this has been interpreted as signifying a qualitative change in the occupation of electronic states,[46] it could also be due to a symmetry breaking.[47] If symmetry breaking is involved, additional phase boundaries should exist in the neighborhood of the point where the H-A line appears to terminate. This

region of the phase diagram needs to be examined in greater detail in order to establish all the phase boundaries. The BSP line, on the other hand, does involve a symmetry breaking and could, in principle, correspond to the ADP-AOP transition.

In conclusion, we have shown that a realistic Hamiltonian for molecular interactions in dense solid hydrogen gives rise to a transition between an orientationally ordered and an orientationally disordered phase, where the order refers to the azimuthal rotational coordinates, at pressures in the range 0.5–2 Mbar. The available information on structural transitions in this range does not permit the unambiguous identification of the ADP-AOP transition with either the BSP or the H-A transitions that have been observed experimentally. Alternatively, the ADP-AOP line may correspond to an unidentified transition which remains to be found experimentally. The strong breaking of the symmetry in this transition should make it easily identifiable by infrared or Raman spectroscopy. We expect that at least a new infrared line should appear when the AOP is obtained due to the breaking of symmetry.[47]

ACKNOWLEDGMENTS

[1] For a review of low-pressure work see I.F. Silvera, Rev. Mod. Phys. **52**, 393 (1980).

[2] I.F. Silvera, Arkhimedes **2**, 108 (1992).

[3] E. Wigner and H.B. Huntington, J. Chem. Phys. **3**, 764 (1935).

[4] D.M. Ceperley and B.J. Alder, Phys. Rev. B **36**, 2092 (1987).

[5] N.W. Ashcroft, Phys. Rev. Lett. **21**, 1748 (1968).

[6] D.A. Papaconstantopoulos and B.M. Klein, Ferroelectrics **16**, 307 (1977).

[7] B.I. Min, H.J. Jansen, and A.J. Freeman, Phys. Rev. B **30**, 5076 (1984).

[8] T.W. Barbee III, A. Garcia, and M.L. Cohen, Nature **340**, 369 (1989).

[9] H.E. Lorenzana, I.F. Silvera, and K.A. Goettel, Phys. Rev. Lett. **63**, 2080 (1989).

[10] H.E. Lorenzana, I.F. Silvera, and K.A. Goettel, Phys. Rev. Lett. **64**, 1939 (1990).

[11] H.E. Lorenzana, I.F. Silvera, and K.A. Goettel, Phys. Rev. Lett. **65**, 1901 (1990).

[12] J.H. Eggert, F. Moshary, W.J. Evans, H.E. Lorenzana, K.A. Goettel, I.F. Silvera, and W.C. Moss, Phys. Rev. Lett. **66**, 193 (1991).

[13] I.F. Silvera, S.J. Leon, and H.E. Lorenzana, Phys. Rev. B **46**, 5791 (1992).

[14] H.K. Mao, P.M. Bell, and R.J. Hemley, Phys. Rev. Lett. **55**, 99 (1985).

[15] R.J. Hemley and H.K. Mao, Phys. Rev. Lett. **61**, 857 (1988).

[16] R.J. Hemley and H.K. Mao, Science **249**, 391 (1990).

[17] H.K. Mao, R.J. Hemley, and M. Hanfland, Phys. Rev. Lett. **65**, 484 (1990).

[18] R.J. Hemley, H.K. Mao, and J.F. Shu, Phys. Rev. Lett. **65**, 2670 (1990).

[19] M. Hanfland, R.J. Hemley, and H.K. Mao, Phys. Rev. B **43**, 8767 (1991).

[20] M. Hanfland, R.J. Hemley, H.K. Mao, and G.P. Williams, Phys. Rev. Lett. **69**, 1129 (1992).

[21] N.W. Ashcroft, in *Molecular Systems Under High Pressure*, edited by R. Pucci and G. Piccitto (Elsevier, Amsterdam, 1991), pp. 201–222.

[22] T.W. Barbee III, A. Garcia, M.L. Cohen, and J.L. Martins, Phys. Rev. Lett. **62**, 1150 (1989).

[23] A. Garcia, T.W. Barbee III, M.L. Cohen, and I.F. Silvera, Europhys. Lett. **13**, 355 (1990).

[24] H. Chacham and S.G. Louie, Phys. Rev. Lett. **66**, 64 (1991).

[25] E. Kaxiras, J. Broughton, and R.J. Hemley, Phys. Rev. Lett. **67**, 1138 (1991).

[26] E. Kaxiras and J.Q. Broughton, Europhys. Lett. **17**, 151 (1992).

[27] N.W. Ashcroft, Phys. Rev. B **41**, 10963 (1990).

[28] D. Hohl, V. Natoli, D.M. Ceperley, and R.M. Martin, Phys. Rev. Lett. **71**, 541 (1993).

[29] H.K. Mao, A.P. Jephcoat, R.J. Hemley, L.W. Finger, C.S. Zha, R.M. Hazen, and D.E. Cox, Science **239**, 1131 (1988).

[30] W. Kohn and L.J. Sham, Phys. Rev. **140**, A1133 (1965).

[31] We use the exchange-correlation expression of J. Perdew and A. Zunger, Phys. Rev. B **23**, 5048 (1984), which is a parametrization of the exact quantum Monte Carlo results of D. M. Ceperley and B.J. Alder, *ibid.* **34**, 2092 (1987).

[32] See, for example, J. Van Kranendonk, *Solid Hydrogen* (Plenum, New York, 1983).

[33] R.P. Feynman and A.R. Hibbs, *Quantum Mechanics and Path Integrals* (McGraw-Hill, New York, 1965).

[34] See B.J. Berne and D. Thirumalai, Annu. Rev. Phys. Chem. **37**, 401 (1986), and references therein.

[35] H. Nagara and T. Nakamura, Phys. Rev. Lett. **68**, 2468 (1992).

[36] R.J. Hemley *et al.*, Phys. Rev. B **42**, 6458 (1990).

[37] D.R. Nelson and B.I. Halperin, Phys. Rev. B **21**, 5312 (1980).

[38] R. Bruinsma and D.R. Nelson, Phys. Rev. B **23**, 402 (1981).

[39] J.V. Selinger and D.R. Nelson, Phys. Rev. A **39**, 3135 (1989).

[40] K.J. Runge, M.P. Surh, C. Mailhiot, and E.L. Pollock, Phys. Rev. Lett. **69**, 3527 (1992).

[41] I.F. Silvera, Science **247**, 863 (1990); H.K. Mao and R.J. Hemley, *ibid.* **247**, 863 (1990).

[42] A.L. Ruoff and C.A. Venderborgh, Phys. Rev. Lett. **66**, 754 (1991).

[43] R.J. Hemley, M. Hanfland, and H.K. Mao, Nature **350**, 488 (1991).

[44] M.P. Suhr, T.W. Barbee III, and C.M. Mailhiot, Phys. Rev. Lett. **70**, 4090 (1993).

[45] I.F. Silvera, Fiz. Nizk. Temp. **19**, 449 (1993) [Sov. J. Low Temp. Phys. **19**, 628 (1993)].

[46] M. Hanfland, R.J. Hemley, and H.K. Mao, Phys. Rev. Lett. **70**, 3760 (1993).

[47] R.M. Martin, V. Natoli, and R. Zallen have recently analyzed this possibility from symmetry-breaking considerations (unpublished).
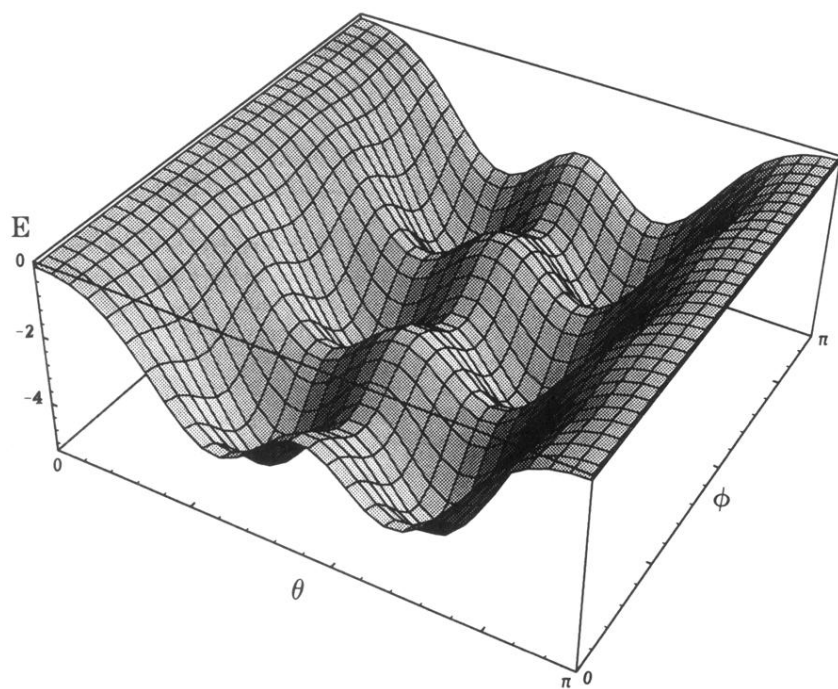
FIG. 14. A two-variable plot of the energy variation as a function of polar and azimuthal angles for the molecular hcp lattice at volume $3.3 \text{ cm}^3/\text{mol}$.